

## RESEARCH ARTICLE

# Global Positioning System precipitable water vapour (GPS-PWV) jumps before intense rain events: A potential application to nowcasting

Luiz F. Sapucci<sup>1</sup>  | Luiz A. T. Machado<sup>1</sup> | Eniuce Menezes de Souza<sup>2</sup> | Thamiris B. Campos<sup>3</sup>

<sup>1</sup>Centro de Previsão de Tempo e Estudos Climáticos, Instituto Nacional de Pesquisas Espaciais, Cachoeira Paulista, Brazil

<sup>2</sup>Departamento de Estatística, Universidade Estadual de Maringá, Maringá, Brazil

<sup>3</sup>Programa de Pós-Graduação em Meteorologia, Instituto Nacional de Pesquisas Espaciais, São José dos Campos, Brazil

## Correspondence

Luiz F. Sapucci, Instituto Nacional de Pesquisas Espaciais (INPE) (CPTEC), Rodovia Presidente Dutra, km 40. CEP: 12630-000. Cachoeira Paulista, São Paulo, Brazil.  
Email: luiz.sapucci@inpe.br

## Funding information

Fundação de Amparo à Pesquisa do Estado de São Paulo, Grant/Award Number: 2009/15235-8, 2015/14497-0; and the Contractual Instrument of the Thematic Network of Geotectonic Studies (CT-PETRO) between PETROBRAS and INPE, Grant/Award Number: 600289299

A rapid increase in atmospheric water vapour is a fundamental ingredient for many intense rainfall events. High-frequency precipitable water vapour (PWV) estimates (1 min) from a Global Positioning System (GPS) meteorological site are evaluated in this paper for intense rainfall events during the CHUVA Vale field campaign in Brazil (November and December 2011) in which precipitation events of differing intensities and spatial dimensions, as observed by an X-band radar, were explored. A sharp increase in the GPS-PWV before the more intense events was found and termed GPS-PWV “jumps.” These jumps are probably associated with water vapour convergence and the continued formation of cloud condensate and precipitation particles. A wavelet correlation analysis between the high temporal-resolution GPS-PWV time series and rainfall events evaluated in this study shows that there are oscillations in the PWV time series correlated with the more intense rainfall events. These oscillations are on scales related to periods from about 32 to 64 min (associated with GPS-PWV jumps) and from 16 to 34 min (associated with positive pulses of the PWV). The GPS-PWV time-derivative histogram for the time window before the rainfall event reveals different distributions influenced by positive pulses of the GPS-PWV (derivative > 9.5 mm/hr) for higher intensity and extension events. These features are indicative of the occurrence of intense precipitation and, consequently, have the potential for application in nowcasting activities.

## KEYWORDS

nowcasting, PWV-GPS, PWV jumps, severe precipitation

## 1 | INTRODUCTION

The application of the Global Positioning System (GPS) tropospheric-induced signal delay to estimate the precipitable water vapour (PWV) (hereafter, GPS-PWV) is a good example of an indirect solution for quantifying atmospheric humidity. The magnitude of this delay is related to the integral of the refractivity index of the air as a function of temperature, pressure and water vapour (Bevis *et al.*, 1992) on the optical path followed by the GPS signal. The wet component of this delay provides the PWV (Bevis *et al.*, 1994),

with an error of approximately 5% under all weather conditions (Wolfe and Gutman, 2000) relative to other measurement techniques (Sapucci *et al.*, 2007) and in near real time (Rocken *et al.*, 1994). The methodology employed in GPS data processing has been continual improvement to minimize the uncertainty, and the PWV estimate has been determined with accuracy > 2 mm (Moore *et al.*, 2015; Shangguan *et al.*, 2015). Although the vertical humidity structure is not captured in GPS-PWV estimates, the great advantage of the GPS-PWV (in addition to its all-weather capacity) is its high temporal resolution of the order of

minutes (Zumberge *et al.*, 1997). An important application of the GPS-PWV estimate is its assimilation into the Numerical Weather Prediction process, which has a positive impact on short-range forecasts of humidity fields and, consequently, better precipitation forecasts for heavy rainfall events (Cucurull *et al.*, 2004; Bennitt and Jupp, 2012). Several applications become viable in dense networks and transects as, for instance: studying the diurnal cycle of convective instability (Sato and Kimura, 2005); studying the water vapour diurnal cycle (Bock *et al.*, 2008); and tracking water vapour advection (Adams *et al.*, 2011). In addition, the GPS-PWV has been employed to provide water vapour tomography to the study of a mistral/sea breeze event in southeastern France (Bastin *et al.*, 2005), as well as to investigate the water vapour distribution of a convective rainfall event (Brenot *et al.*, 2014). The GPS-PWV was also employed for nowcasting studies by Jerrett and Nash (2001) using the GPS signal to nowcast thunderstorm activities; by Kursinski *et al.* (2008) and Benevides *et al.* (2015) by evaluating the GPS-PWV's behaviour before precipitation; and by Serra Yolande *et al.* (2016) to study mesoscale convective events during the North American Monsoon. Guerova *et al.* (2016) discuss the importance of the GPS-PWV high time-resolution and provide a detailed humidity observation for severe weather nowcasting.

The relationship between the occurrence of intense rainfall and high concentrations of atmospheric water vapour is well known and has been studied for well over a decade. Muller *et al.* (2009), using a simple two-layer model, discuss the precipitation–humidity relationship in the Tropics. Holloway and Neelin (2010) employed PWV data from a microwave radiometer with high temporal resolution (6 min) to study the relationship and variability between the column water vapour and precipitation. Chan (2009) evaluated the performance of a ground-based microwave radiometer in intense convective weather events and reported an increasing degree of instability of the Troposphere before the occurrence of heavy rain. Madhulatha *et al.* (2013) reported a sharp increase in the PWV values approximately 2–4 hr before the occurrence of thunderstorms and developed a nowcasting technique using PWV values and seven other thermodynamic indices from microwave radiometer observations. Mazany *et al.* (2002) developed a lightning prediction index for Florida based on the GPS-PWV magnitude and its temporal evolution. This index was designed using a binary logistic regression model-based PWV-GPS and other two variable predictors. The GPS lightning index time series showed a typical pattern several hours before a lightning event. Haan *et al.* (2004) demonstrated the viability of the use of the GPS-PWV combined with satellite imaging to improve thunderstorm and heavy precipitation forecasts during the passage of a cold front. Haan (2006) developed a method for inferring the atmospheric stability from a non-isotropic

GPS path-delay signal (slant delay). This large lead time, around 2–3 hr, is probably related to large-scale convergence and not to the convective-scale process because clouds have a shorter life cycle. More recently, Adams *et al.* (2013) used 3.5 years of Amazon GPS-PWV to study the use of the GPS to derive a water vapour convergence timescale associated with the shallow-to-deep convective transition. Benevides *et al.* (2015) analysed the temporal behaviour of the GPS-PWV time series in a number of case studies of intense precipitation in the Lisbon area of Portugal.

Considering the 1 hr lead time associated with convective clouds, the near real-time GPS-PWV data could, in principle, be employed as a nowcasting tool for intense rainfall events. Considering the PWV's variability before deep convective precipitation events, probably related to water vapour convergence, the GPS can be used for nowcasting if the variability before a rainfall event is well known. The motivation of the present study is to evaluate this variability and relationship with rainfall, focusing specifically in the high-resolution GPS time-scale data to evaluate the rapid increases in the PWV (hereafter termed the GPS-PWV jump) before the onset of deep convective rainfall events.

The paper is structured as follows. Section 2 presents the data collected during the CHUVA Vale experiment in Brazil and describes the GPS data-processing technique for obtaining PWV values. An X-band radar was used to quantify the spatial-temporal distribution of the precipitation events. Section 3 defines and characterizes the GPS-PWV jumps. Section 4 presents the high temporal-resolution GPS-PWV time-series analysis, including wavelet analysis and time-lag correlations between the precipitation and the GPS-PWV time series, as well as the evaluation of the GPS-PWV derivatives before precipitation events of different extensions. Section 5 concludes.

## 2 | DATA COLLECTION DESIGN AND PROCESSING METHOD

The data employed in this study were collected during the CHUVA Vale campaign, one of the field campaigns of the CHUVA project (Machado *et al.*, 2014). The CHUVA project was designed to investigate cloud microphysical and precipitation processes through six intensive field campaigns covering various precipitation regimes in Brazil. The campaign was carried out in São José dos Campos City in São Paulo state (23 ° 12 ' 30 " S and 45 ° 57 ' 08 " W) in an elevated valley between the Mantiqueira and Serra do Mar mountain ranges. Figure 1 shows the geographical location of the CHUVA Vale campaign. This region is dominated by deep convection with typical rainfall systems that are forced by sea breeze–mountain convergence zones as well as squall

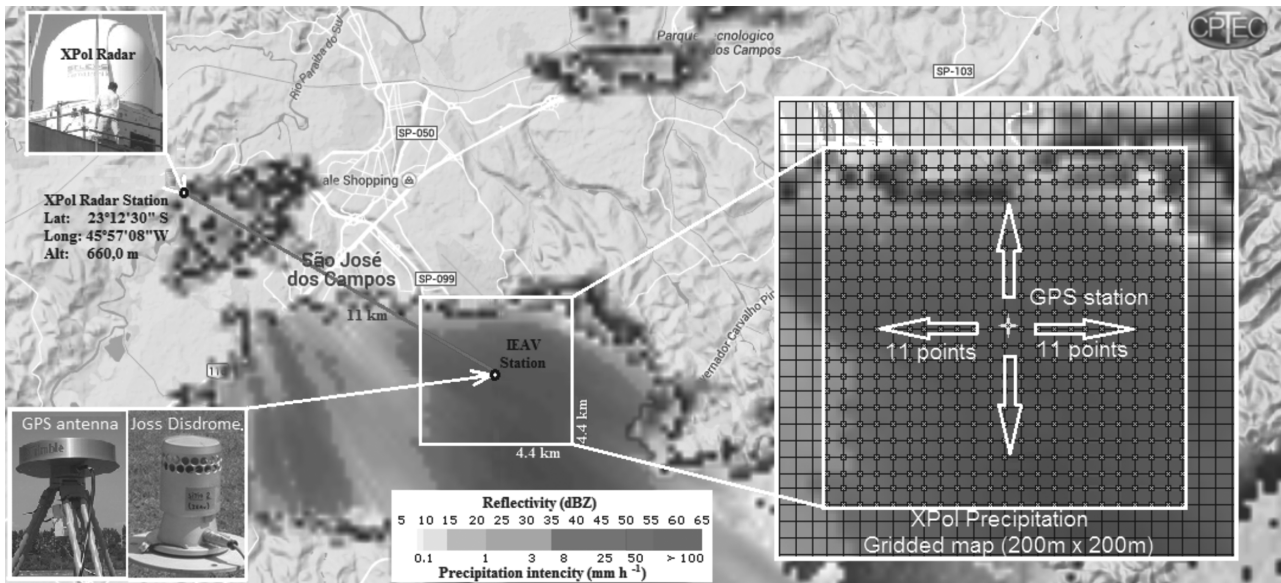


**FIGURE 1** The CHUVA Vale experiment in which the sites where the XPol radar, Global Positioning System (GPS) receiver and disdrometer were installed are indicated. The area of  $4.4 \times 4.4$  km around the GPS station is highlighted in this figure over the precipitation field observed by XPol radar on December 14 (DoY 348) 2011. Some details about the composition of this area using the points of the XPol gridded map are additionally presented

lines associated with cold front penetration (Machado *et al.*, 2014).

## 2.1 | Data from the CHUVA Vale experiment

The experiment consisted of an intensive observation period between November 3 and December 28, 2011. The instruments used were a dual-frequency GPS receiver for scientific applications, a disdrometer and a mobile X-band dual polarization radar (XPol). The TRIMBLE brand GPS receiver, model NETR8 with Dorne-Margolin Choke Ring antenna, used was installed 11 km from the XPol radar at the site nominated by the Institute of Advanced Studies (the IEAV site). Any sky obstructions around the GPS receiver were avoided to minimize the multi-path effect in GPS signal propagation. See Figure 1 for more details about the sites at which the instruments were placed.

The GPS satellite signals were sampled at 1 s frequencies, whereas the collocated meteorological sensor captured the pressure and temperature at 1 min frequencies. A Joss-Waldvogel brand acoustic impact disdrometer (Joss and Waldvogel, 1967), model RD 80, was installed a few metres from the GPS receiver. The XPol radar scan strategy collected one volume scan every 6 min at 13 elevations, from  $1^\circ$  to  $25^\circ$ , with  $1^\circ$  and 150 m angular and radial resolutions respectively. Owing to a technical problem, the radar was turned off between 1236 UTC on November 14 and 1941 UTC on November 15. The radar data were pre-processed using the attenuation correction of the reflectivity, employing the algorithm for ground-based polarimetric radars (ZPHI algorithm) proposed by Testud *et al.* (2000). For a detailed description of the radar and disdrometer pre-processing, see Calheiros and Machado (2014).

## 2.2 | High temporal-resolution GPS-PWV time series

The zenith total delay (ZTD) was obtained by processing the GPS data using GOA-II (Gipsy, GPS Inferred Positioning System; OASIS, Orbit Analysis and Simulation Software II; Gregorius, 1996) software by applying the precise point-positioning method in post-processing mode with the precise ephemeris of the GPS constellation provided by the NASA Jet Propulsion Laboratory (JPL). The sampling rate of the used GPS satellites ephemeris is 15 min for orbits and 5 min for the GPS satellite clock.

To ensure the quality of the PWV time series with the high temporal resolution required for this study, in the data-processing strategy adopted the known uncertainty sources were taken into consideration by applying the recommended models and adjusting the parameter exploring the available stochastic models. The latest version of the GOA-II software (v. 6.3) was used: it adjusts parameters with high temporal resolution by exploring the sophisticated orbit integrator package to estimate the GPS satellite position in each epoch. The ocean tide model FES 2004 (Lyard *et al.*, 2006), recommended by the International Earth Rotation and Reference Systems Service (IERS Conventions, 2010), was applied in this processing. A method of antenna absolute calibration (Schmid *et al.*, 2007) was applied by GOA-II to ensure the correct phase centre variation of the satellites and receiver antennas using parameters provided by the International GNSS Service (IGS) website (Montenbruck *et al.*, 2015). The data processing with GOA-II software to obtain ZTD estimates was performed by selecting the global mapping function (Boehm *et al.*, 2006) and the sampling rate of the ZTD estimates of 60 s. The parameters employed to estimate the ZTD are listed in Table 1.

**TABLE 1** Configuration items associated with zenith total delay (ZTD) estimates and respective values used in the Global Positioning System (GPS) data processing using GOA-II software

Configuration item	Parameter used	Comments
GPS data file for GOA-II	Rinex format in a sampling rate of 1 s	Data collection from CHUVA
Mapping function	Global Mapping Function (Boehm <i>et al.</i> , 2006)	Selected in the data processing
Cut-off elevation angle	10°	Selected in the data processing
Elevation-dependent inverse weights ( $\sigma^2 =$ )	1/sin(e)	Suggested by JPL
<i>A priori</i> zenith delay	From the GPT2 model	Suggested by JPL
<i>A priori</i> meteorological source and mapping coefficients	GPT2 for pressure, temperature, relative humidity and GPT2 mapping function coefficients	Suggested by JPL
Mapping of <i>a priori</i> zenith delay to the line of sight	Slant dry plus wet delays mapped with GPT2	Suggested by JPL
Mapping function used for zenithal delay adjustment	GPT2 wet mapping function; the ZWD is estimated at each epoch as a random walk with process noise of $0.05 \text{ mm sqrt(s)}^{-1}$	Suggested by JPL
Estimate of North–South and East–West tropospheric gradients	Estimated at each epoch as a random walk with process noise of $0.005 \text{ mm sqrt(s)}^{-1}$	Suggested by JPL
Sampling rate of the ZTD estimates	60 s	Selected in the data processing

Note. GPT2, Global Pressure and Temperature model-Version 2; JPL, Jet Propulsion Laboratory; ZWD, Zenithal Wet Delay.

The zenith wet delay was obtained from the ZTD after removing the zenith hydrostatic delay obtained by the application of a representative tropospheric temperature model and a surface pressure measurement (Davis *et al.*, 1985). The zenith wet delay was converted to the PWV by using the relationship suggested by Bevis *et al.* (1992). The mean tropospheric temperatures with a sampling rate of 1 min were obtained from the temperature and pressure measured at the GPS antenna by applying the regional model suggested by Sapucci (2014), which is the most suitable for this region. The sampling rate of the GPS-PWV values was 1 min. The GPS-PWV time series suffered some short failures due to interruptions in data collection. These time-series interruptions occurred in 3,183 epochs (3.1% of the total period), and the missing values were filled by a cubic spline interpolation method specific for the application of wavelet analysis, which requires complete time series without failures. These interpolations were concentrated within two specific days of year (DoY) (331 and 348), and these periods with PWV interpolated values were not employed in the data analysis.

### 2.3 | Precipitation time series from a disdrometer and XPol radar data

The reason for choosing a disdrometer to quantify the precipitation is that this instrument provides an instantaneous measurement of the rainfall intensity (mm/hr) at the same GPS-PWV sampling rate; however, this information is only representative of a very small spatial scale (a sampling area of  $50 \text{ cm}^2$ ). Notably, the XPol radar data generate information with a different and more representative spatial resolution around the GPS receiver.

The precipitation rates were obtained from the Joss disdrometer data by applying the methodology suggested by Kinnell (1976), in which the precipitation intensity of each 1 min is inferred from the size and concentration of the rain drops observed during this period. The precipitation data

from the XPol radar observation were obtained by applying the dual polarization surface rainfall intensity algorithm, which calculates the rainfall rate ( $R$ ) from the reflectivity ( $Z$ ) and specific differential phase data obtained in multiple-elevation polar volumes. In this method, polarimetric measurements are used to calculate  $R$  by applying a combined  $Z$ – $R$  relationship (Bringi *et al.*, 2005). The final product of this process is a gridded map (60 km radius around the XPol radar) with a horizontal resolution of 200 m, in which each grid point value for rainfall intensity (mm/hr) at a sampling rate of 6 min is available.

Several options exist for the selection of the rainfall area used to calculate the time series of the precipitation fraction observed by the radar which is then combined with the GPS-PWV. The rainfall area can be selected as that with the highest correlation between the GPS-PWV and the rainfall, even considering a lag among the two measurements, as will be demonstrated below. The selected area for this study was  $4.4 \times 4.4 \text{ km}$  (approximately  $20 \text{ km}^2$ ) around the GPS antenna, which corresponds to  $22 \times 22$  radar pixels centred on the GPS's position. Although this area does not exactly match the cone of the GPS observation, it presented the highest correlation with the rainfall area fraction. The rainfall area employed in this study is only a reference for the description of the GPS-PWV and rainfall relationship. Figure 1 shows the configuration of the XPol radar, GPS antenna and disdrometer in the CHUVA Vale experiment and highlights the selected area. The precipitation field observed by XPol on December 14, 2011 (DoY 348) is also presented to illustrate the points from the XPol gridded map used to represent the precipitation area around the GPS antenna taken into account in this study. This event was chosen because it was the most intense, with 70% of the area around the GPS antenna recording precipitation  $> 50 \text{ mm/hr}$ .

As the focus here is to study the GPS-PWV behaviour during intense rainfall, the statistical measurements calculated from the radar data were for the case studies at the 95th

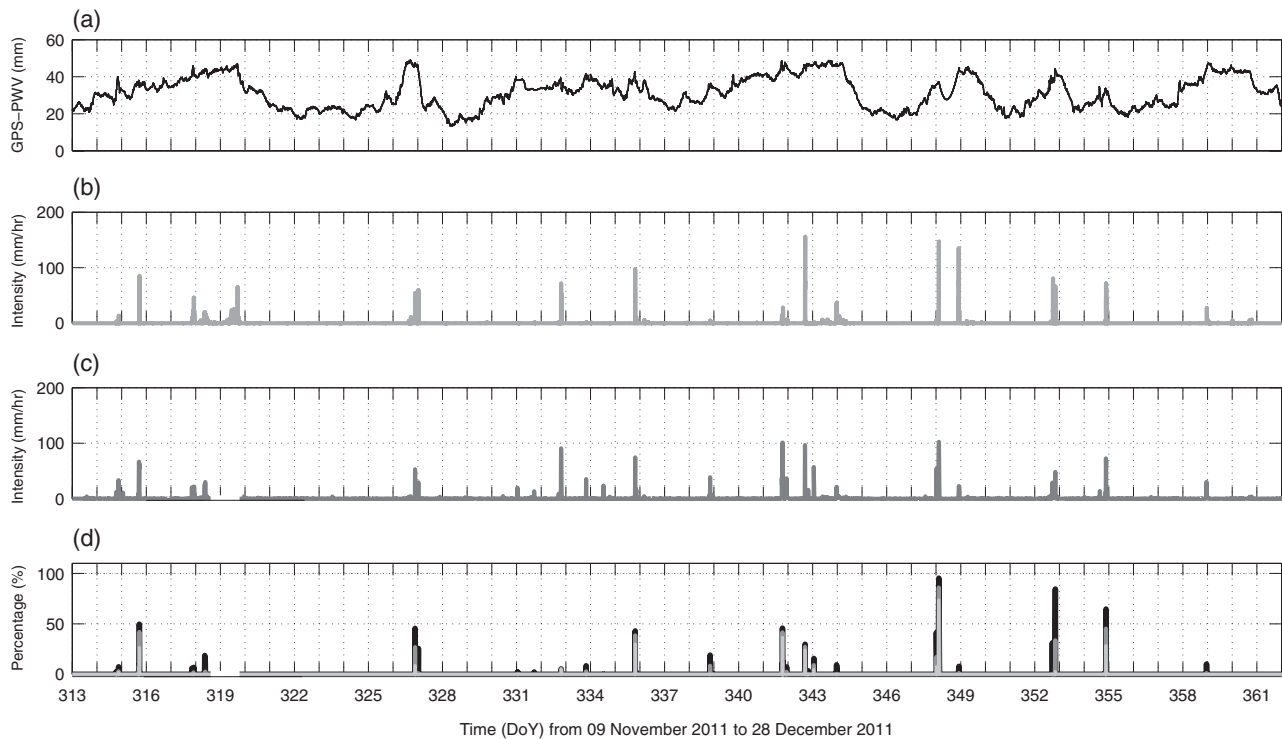


**FIGURE 2** Time series of the precipitation and Global Positioning System precipitable water vapour (GPS-PWV) obtained during the CHUVA Vale campaign (from 09 November to 28 December 2011): (a) GPS-PWV time series; (b) precipitation intensity observed by a Joss disdrometer; (c) 95th percentile of the precipitation intensity observed by XPol radar in the area of  $4.4 \times 4.4$  km centred on the GPS antenna; and (d) precipitation fraction in the area of  $4.4 \times 4.4$  km centred on the GPS antenna, where the black bar is the fraction  $> 20$  mm/hr, the dark grey bar is the fraction  $> 35$  mm/hr and the light grey bar is the fraction  $> 50$  mm/hr

percentile of the intensity of the precipitation observed in the selected area. Additionally, to evaluate rainfall events of different intensities, the rain fraction was computed as the fraction of area of  $4.4 \times 4.4$  km around the GPS antenna with precipitation rates above some chosen threshold. The first approach emphasizes the more intense localized precipitation events; the second simultaneously quantifies the intensity and extension of each event. The chosen thresholds to compute the rain fraction considered the following intensities: moderate to heavy ( $> 20$  mm/hr), heavy to intense ( $> 35$  mm/hr) and intense to torrential ( $> 50$  mm/hr). The disdrometer was used only for a reference and for comparison with the radar rainfall estimations. Figure 2 presents time series for the GPS-PWV (Figure 2a), the precipitation from the disdrometer data (Figure 2b) and, from the XPol radar, the 95th percentile of the precipitation intensity (Figure 2c) and the rain fractions for different thresholds (Figure 2d). The period studied was from November 9 (DoY 313) to December 28 (DoY 362), 2011, during which the GPS receiver, XPol radar and disdrometer were simultaneously collecting data. Figure 2 shows that the disdrometer time series is consistent with the 95th percentile time series, although differences are expected due to the different areas covered by each instrument, and besides, the total precipitation from the disdrometer is always larger than that measured by radar and a rain gauge because large droplets were not filtered as suggested by Giangrande *et al.* (2016).

### 3 | BEHAVIOUR OF THE PWV TIME SERIES BEFORE PRECIPITATION EVENTS: THE GPS-PWV JUMPS

The high temporal resolution obtained with the GPS-PWV enables the evaluation of high-frequency variations and their relationship with intense precipitation events. The GPS-PWV time series shows a well-defined sharp increase before the occurrence of precipitation, as reported by Kursinski *et al.* (2008) as a rapid rise in the PWV preceding the rain events. Shi *et al.* (2015), when using the GPS-PWV to monitor water vapour variation, showed that ascending and descending patterns of the GPS-PWV can be identified before and after each rainfall event. Benevides *et al.* (2015), in a case study, reported that severe rain events occurred just after the largest GPS-PWV peak. There are strong oscillations generating a significant increase in the total water vapour content until a maximum is reached. Subsequently, a strong GPS-PWV reduction is observed, and after a short interval, the precipitation also reaches a maximum peak. This sharp increase in the GPS-PWV values before the occurrence of more intense rainfall events is GPS-PWV jump. The GPS-PWV time series was evaluated using wavelet analysis in a study of correlation and lags with rainfall events to form a conceptual model with predictive capacity, which can be useful as a nowcasting tool for strong precipitation events.

Figure 3 shows a typical case exemplifying the PWV behaviour before precipitation occurs on DoY 341; this was one of the strongest events registered during the CHUVA Vale experiment. Before the severe precipitation begins, the GPS-PWV follows several positive pulses, increasing the value and forming the GPS-PWV jump, until it reaches a peak of maximum value. These pulses are in a temporal scale lower than the PWV jump, which can be identified by differences between PWV values (pulses in the PWV), shown in the inset in Figure 3 (shown by vertical arrows). After the GPS-PWV crest, a decreasing period is observed some minutes before severe precipitation. Figure 3 clearly shows this configuration of a crest in the GPS-PWV time series around precipitation (composed of several pulses) and its subsequent decrease immediately before the beginning of stronger precipitation.

This GPS-PWV behaviour before precipitation occurs not only for more intense events but also for lower rainfall

rates. Figure 4 shows that other GPS-PWV jumps observed before rain events with different intensity/extension occurred on DoY 315 (41% of precipitation fraction > 35 mm/hr), DoY 333 (2%) and DoY 358 (only 1% of precipitation fraction > 35 mm/hr). Figure 4 shows the intensity of these sharp increases in the GPS-PWV are larger before more extensive precipitation. Table 2 presents all precipitation events in which rainfall > 20 mm/hr was observed by the XPol radar in the area of  $4.4 \times 4.4$  km around the GPS antenna. Table 2 also presents the DoY and time of maximal radar precipitation of each event and the respective fraction rain > 20, 35 and 50 mm/hr. To obtain an overview of the hardness of the GPS-PWV jumps feature before precipitation, Figure 5 show the composite mean of the GPS-PWV time series from 60 min before to 60 min after the maximum observed precipitation (fraction rain > 35 mm/hr) for the 18 events listed by Table 2. The composite presented shown in Figure 5 is normalized by maximum GPS-PWV values

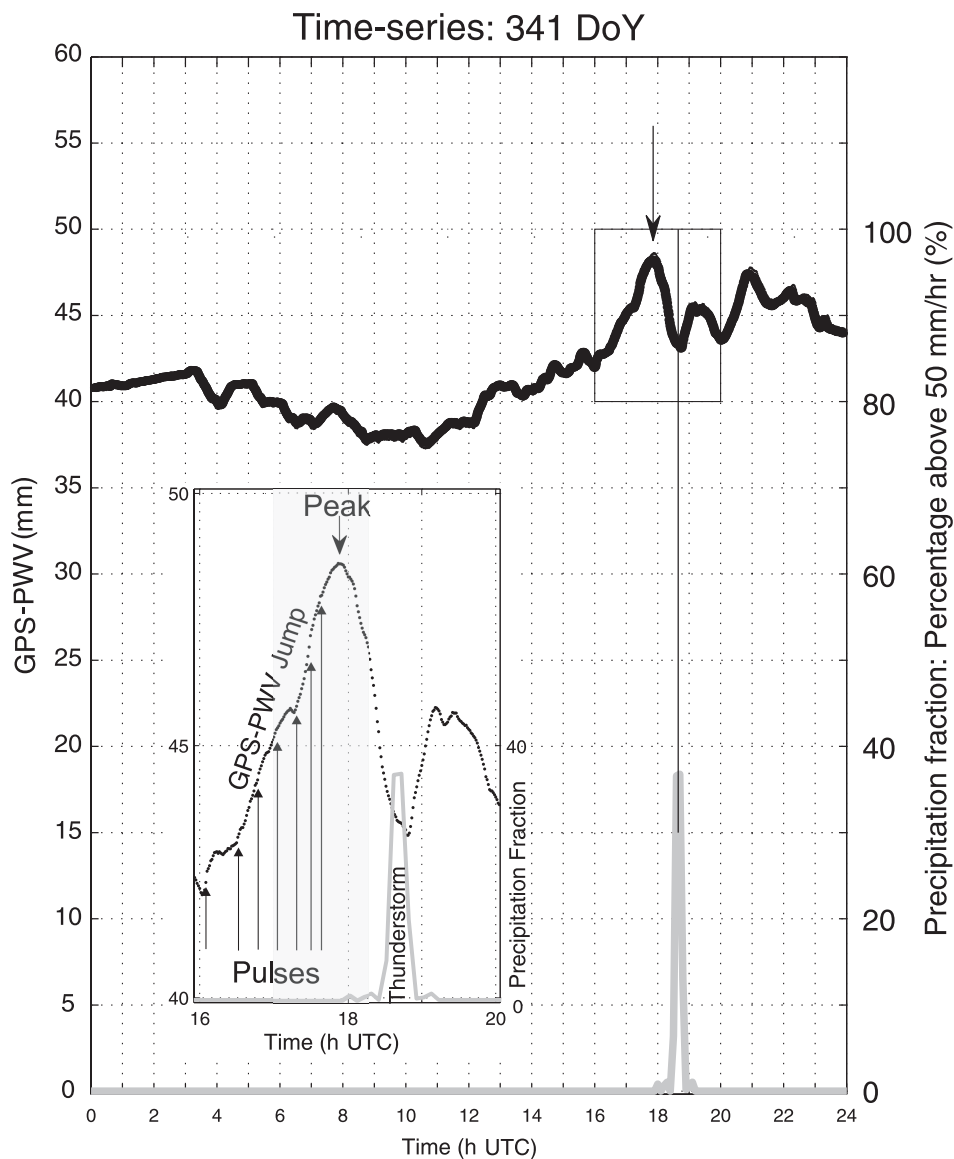


**FIGURE 3** The Global Positioning System precipitable water vapour (GPS-PWV) jump observed in the 2 hr period before a heavy storm that occurred during day of year (DoY) 341 (December 7, 2011, 1836 UTC)

before precipitation. The composite mean shows that the GPS-PWV jump is strongly remarkable before the maximum precipitation, in which the maximum of the composite mean is observed in 30 min and lower dispersion in 25 min before the maximum precipitation. The time lag between the maximum GPS-PWV and the time of the maximum rainfall is presented as an inset in Figure 5. In this histogram, it is clear there is a range of lag time between the GPS-PWV and precipitation maximums. The precipitation area and the temporal resolution of the GPS-PWV here employed have an impact on this lag time. For instance, Adams *et al.* (2013), when using a rain gauge and the PWV with a sampling rate of 30 min over the Amazonian region, found a zero lag. However, in the present study shows that the GPS-PWV signal can represent a precipitation area and not only a punctual measurement over the GPS antenna. An analysis of the time-lag correlation is necessary to define this interval between the maximal GPS-PWV and precipitation, which is carried out in the next section.

This temporal behaviour of the PWV (GPS-PWV jumps) before the occurrence of intense rain events could be explained by the following physical processes: Lindzen and Tung (1976) showed that water vapour may increase through low-level moisture convergence produced by wave patterns generated by gravity waves forced by the released latent heating in the strong convective process. The variation of the moisture convergence generates a sequence of pulses increasing in the PWV values, similar those shown in Figure 3. Raymond (1987) discusses low-level water vapour convergence forced by a gravity wave, but also discusses others physical mechanisms that induce low-level moisture convergence, as, for instance, unstable surface parcels accelerating upwards by local convergence. Sometime after the crest of the jump, rain reaches its maximum intensity

followed by a decrease of the PWV. A possible reason for the PWV decrease is associated with the conversion process from water vapour to liquid. This conversion changes the dielectric medium, where the refractivity is induced by the displacement of charge (Solheim *et al.*, 1999). While the refractivity from water vapour is due to the polar nature of the water molecule, the GPS phase delay induced by liquid water (hydrometeor) is proportional to the electric permittivity of the formed dielectric medium and, consequently, is much lower than the delay generated by the water vapour. Another physical mechanism that can explain this PWV reduction is the storm downdraft that dries and cools the atmosphere. In addition, the PWV decreases after precipitation starts can be associated with the final process of surface convergence, or simply by the advection process forced by the shear and storm movement. The lag time between the crest and the maximum precipitation can vary from the selected area fraction employed or by the convection type. The precipitation efficiency, normally a function of the wind shear, can play an important role in this feature. Adams *et al.* (2013) considered that the conversion of water vapour to liquid and precipitation are of second order during the process of increasing PWV. It is probably true during the phase of cloud formation, however, when the precipitation starts, that this conversion could be of the first order.

#### 4 | HIGH TEMPORAL-RESOLUTION GPS-PWV TIME-SERIES ANALYSIS

This section explores the high temporal-resolution GPS-PWV time series and precipitation of different intensity and extension and it characterizes the PWV-GPS jumps. The wavelet analysis allows a study to be made of the main time-scale of the GPS-PWV variability and the time-lag

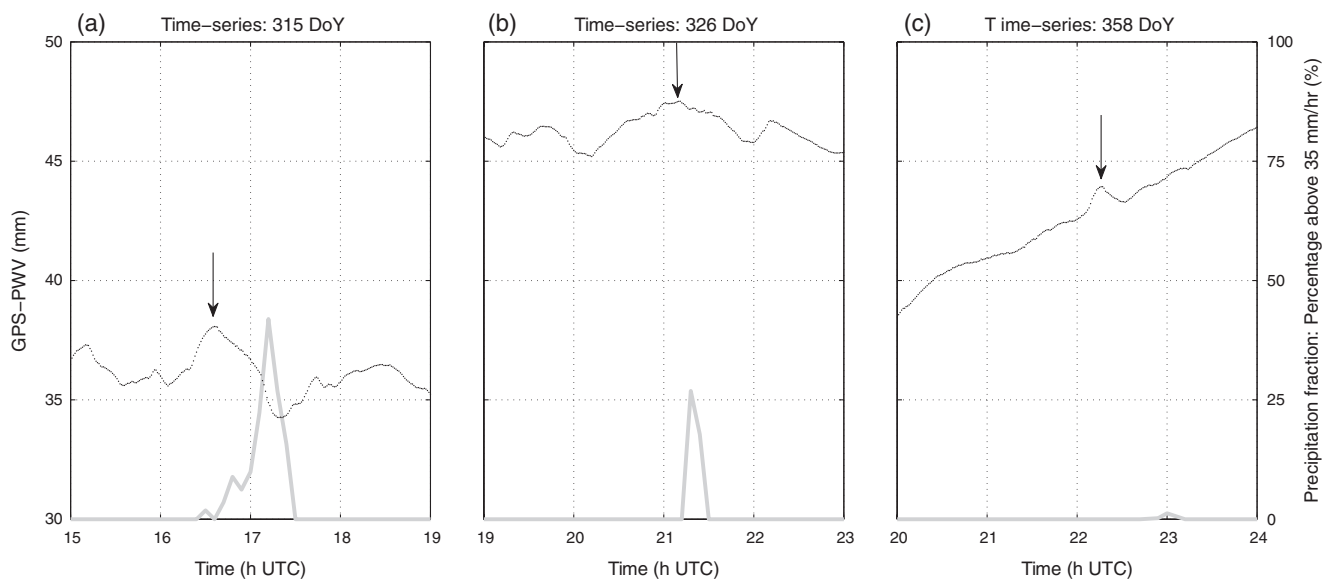


**FIGURE 4** Other cases of Global Positioning System precipitable water vapour (GPS-PWV) jumps observed before precipitation events with a fraction > 35 mm/hr of different extension that occurred during: (a) day of year (DoY) 315 (1712 UTC); (b) 333 DoY (1942 UTC); and (c) 358 DoY (2300 UTC)

**TABLE 2** Precipitation events observed by radar during the CHUVA Vale experiment in different extension terciles as a function of the precipitation fractions > 35 mm/hr

Event	Day of year (DoY)	Maximal radar precipitation UTC time (hhmm)	Precipitation fraction observed by the XPol radar (%)			Terciles
			> 50 mm/hr	> 35 mm/hr	> 20 mm/hr	
1	348	0242	73	85	95	Upper
2	354	2112	28	45	63	Upper
3	341	1836	36	41	45	Upper
4	315	1712	26	41	49	Upper
5	335	1924	30	38	42	Upper
6	352	2000	2	33	84	Upper
7	342	1636	24	27	28	Middle
8	326	2118	8	26	45	Middle
9	343	0106	4	9	15	Middle
10	338	2018	0	8	19	Middle
11	332	1918	5	5	5	Middle
12	333	1942	0	2	8	Middle
13	314	2106	2	2	7	Lower
14	327	0036	0	1	25	Lower
15	358	2300	0	1	10	Lower
16	317	2148	0	1	2	Lower
17	318	0848	0	0	19	Lower
18	331	1712	0	0	2	Lower

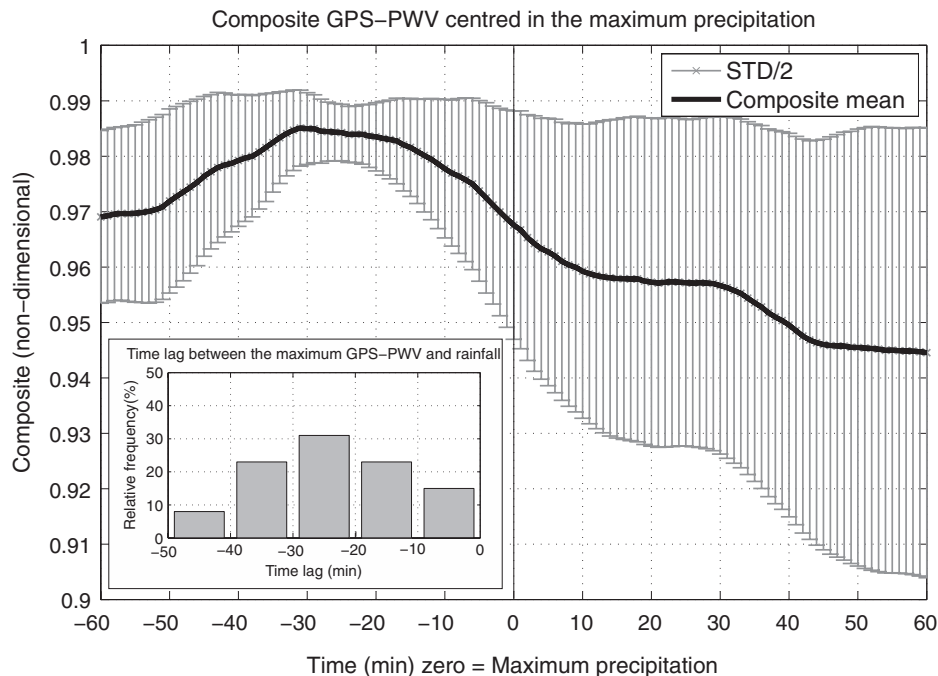


**FIGURE 5** Composite Global Positioning System precipitable water vapour (GPS-PWV) time series 60 min before and 60 min after 18 the precipitation events listed in Table 2, and the distribution of the time lag between the maximum GPS-PWV and the time of the maximum rainfall of these events (precipitation fraction > 35 mm/hr in the area of  $4.4 \times 4.4$  km centred on the GPS)

correlation with rainfall. This section also explores the GPS-PWV time-derivation analysis and its potential for nowcasting application.

#### 4.1 | Wavelet analysis

Wavelet analysis is used to perform a detailed analysis of the GPS-PWV time series and to evaluate the variability

within different timescales (denoted here as intra-relation), as well as to assess the relationship between the GPS-PWV time series and the precipitation time series (denoted here as inter-relation wavelet analysis). This methodology enables simultaneous decomposition of the PWV time series as a function of time and frequency (Daubechies, 1992). Consequently, accessing the information regarding the signal

amplitude/frequency and its variation as a function of time becomes possible. Appendix S1 presents more information about the wavelet analysis and methodology employed in this study. The results obtained in the wavelet power spectrum in an intra-relation analysis of the GPS-PWV and 95th percentile of the precipitation intensity time series are also presented in Appendix S1. The analysis of the wavelet power spectrum during precipitation events indicates the scales evolved in the GPS-PWV jumps events. Note the importance of the 128 to 16 min timescale during more intense precipitation events than during light rainfall events.

Daubechies and least asymmetric wavelets, with different filter lengths (coefficient number), were used in the inter-relation analysis of the GPS-PWV and precipitation. The results were quite similar independently of the mother wavelet, but the correlations were maximized when the mother wavelet has a larger filter or more coefficients. Figure 6 shows the estimated wavelet correlations using the larger filter (LA20 mother wavelet). Figure 6a shows the wavelet correlation and its 95% confidence interval between the GPS-PWV and the 95th percentile of the precipitation intensity as a function of the wavelet scale, represented by the respective time periods, considering the zero lag. In this analysis, the precipitation estimated from the XPol radar, originally with a sampling rate of 6 min, was linearly interpolated to a rate of 1 min. The results show that the positive wavelet correlation between the PWV and precipitation intensity is stronger for the scale related to the period between 32 and 64 min, indicating the scale on which the most important GPS-PWV oscillations associated with precipitation events occur. Larger than this timescale, the correlation decreases, followed by another increase due to the influence of the diurnal cycle. The correlations are not very high, but they are statistically significant at a 95% confidence interval.

To evaluate the results presented in Figure 6a for different intensities and extensions of the precipitation events, the other insets shows the wavelet correlation for zero lag between the GPS-PWV and precipitation fractions as a function of the period bands for different rain fraction intensities ( $> 20$  mm/hr, Figure 6b;  $> 35$  mm/hr, Figure 6c; and  $> 50$  mm/hr, Figure 6d). The 95% percentiles give information about the maximum rain rate (which can be only 1 point) in the area of  $4.4 \times 4.4$  km around the GPS antenna. The rain fraction gives information about the fraction of this studied area covered by a rain rate above these thresholds. There are some events where the rain intensity can be high and the fraction small, for instance, the cases of isolated clouds. Therefore, the area fraction presents a closer representation of rainfall events related to low-level convergence because it gives information about the amount of liquid water in the area. The peak of the wavelet correlation observed in the period from 32 to 64 min is significant for the three rain thresholds. The plots in Figure 6 also show stronger wavelet correlation when only heavy to torrential precipitation events are taken into

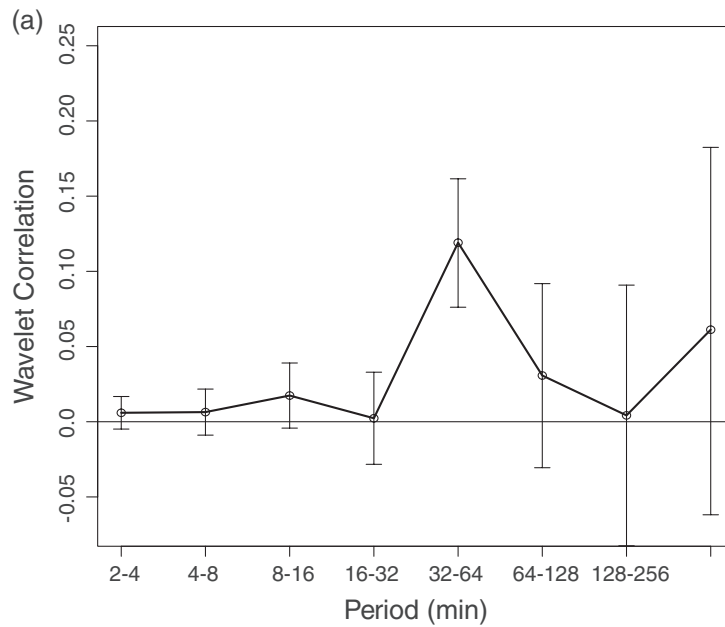
consideration. That signals the occurrence of precipitation events of large intensity and extension, which suggests that the GPS-PWV jumps are concentrated at this scale. It is also important to highlight that the correlation is larger on this scale than on adjacent scales.

To investigate a possible lead-lag time relationship between these time series, the wavelet cross-correlations (WCCs) were estimated for various lags (Whitcher *et al.*, 2000). For simplification, the precipitation threshold of 35 mm/hr was selected in this analysis. Figure 7 shows the WCCs between the GPS-PWV and the percentage of points with precipitation  $> 35$  mm/hr, observed by radar co-located to the GPS antenna, as a function of the lead-lag for different periods. Lower wavelet scales such as 2–4 and 4–8 and 8–16 do not exhibit cross-correlations significantly larger than zero for larger lags (see the grey triangle in the WCC plots). For timescales between 16–32 and 32–64, two positive peaks in the WCC are observed, as indicated by the grey arrows in Figure 7. These peaks are at lags of  $-28$  and  $-12$  min for wavelet scales of 16–32 min periods and lags of  $-30$  and  $-5$  min for 32–64 min periods. Patterns in higher timescales,  $> 64$  min corresponding to the daily trends humidity, present the largest WCC values with a lag of 30 min. Although the precipitation and GPS-PWV time series present very distinct behaviours, the WCC revealed the relationship between wavelets for scales related to time periods from 16–32 to 32–64 min in a lead-lag of about 30 min before the precipitation events. These results obtained by correlation wavelet analysis demonstrate that the GPS-PWV jump is associated with the PWV oscillations in the period 32–64 min. In addition, these results suggest that PWV higher frequency positive pulses that build the PWV jump are within the timescale of 16–32 min.

The wavelet correlation analysis between the GPS-PWV in different timescale and precipitation events emphasizes the potential of this technique to predict intense precipitation events. The GPS-PWV jump occurs before precipitation; however, the intensity of the jump, formed by these positive pulse oscillations, depends on the rainfall rate. Of course, it should have regional variability because the timescale between humidity convergence and rainfall may depend on many physical processes and environmental conditions, as discussed above.

#### 4.2 | Time-lag correlation analysis

The relationship between rainfall intensity (or rain fraction) and the GPS-PWV is different for each event; however, the GPS-PWV peak is a well-delineated pattern. The time interval between the moment of the PWV crest and maximal precipitation can vary between cases. The WCC shows on which scale the correlation between the GPS-PWV and precipitation time series is higher, as well as the lead-lag interrelation between them. However, evaluating the lag correlation for positive and negative correlations is also important for further developing nowcasting tools. Figure 8



Wavelet correlation values between GPS-PWV and percentage of points with observed precipitation by radar around

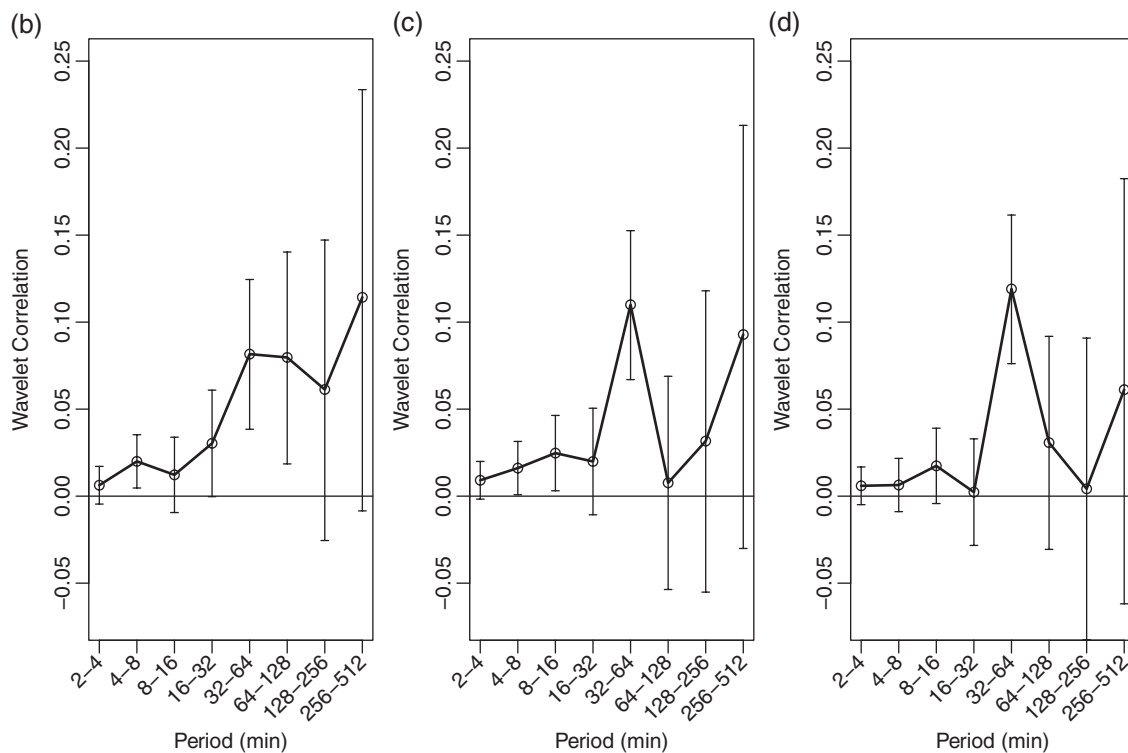


**FIGURE 6** Wavelet correlations between the Global Positioning System precipitable water vapour (GPS-PWV) and precipitation observation time series as a function of the different wavelet scales represented by their respective time periods, in which: (a) is for the 95th percentile of the precipitation intensity from the XPol radar; (b) is the percentage of points  $> 20$  mm/hr observed by radar around the GPS antenna; (c) as for (b), but for  $> 35$  mm/hr; and (d) as for (b), but for  $> 50$  mm/hr. The correlation is estimated by considering the lag zero. The 95% confidence interval for each wavelet cross-correlation (WCC) is estimated by considering a Gaussian distribution after applying the Fisher's Z transformation. Source: Whitcher *et al.* (2000))

shows histograms for the lag correlations (the time lags for the maximum and minimum correlations) between the GPS-PWV and rain fraction for all events in which the rainfall rate observed around the GPS antenna was  $> 20$  mm/hr. The 18 events listed in Table 2 were evaluated, in which different rain fractions were observed using the XPol radar. The

histogram was constructed based on the correlation time lags found for the positive (maximum) and negative correlations (minimum). The search time-lag interval for the positive (negative) correlation was restricted for a period before (after) the precipitation because there were some subsequent rain events very close by that could mislead the results.

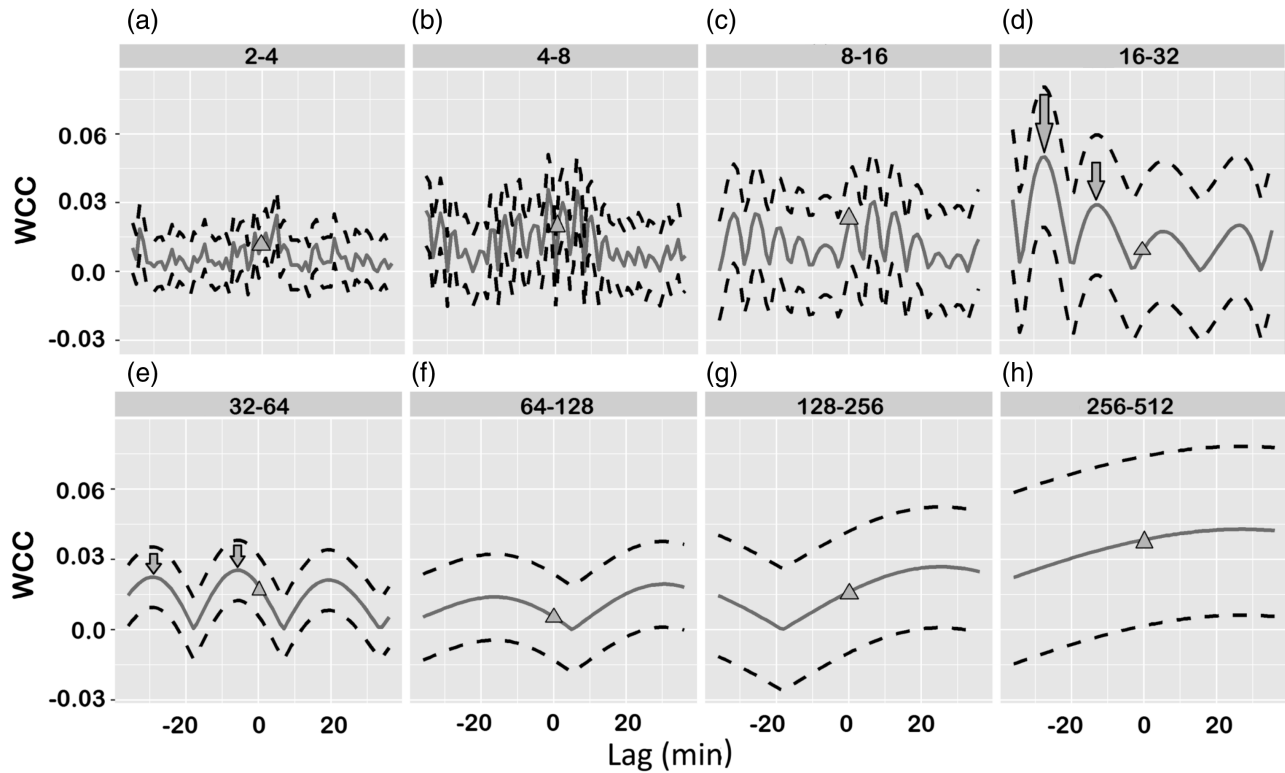


**FIGURE 7** Wavelet cross-correlations (WCCs) between the Global Positioning System precipitable water vapour (GPS-PWV) and percentage of points > 35 mm/hr observed by radar around the GPS antenna as a function of the lead-lag for different time periods (in minutes): (a) from 2 to 4; (b) from 4 to 8; (c) from 8 to 16; (d) from 16 to 32; (e) from 32 to 64; (f) from 64 to 128; (g) from 128 to 256 and (h) from 256 to 512 minutes. The dotted line represents the 95% confidence interval

The type of correlation used in this study was Spearman's  $\rho$  (Best and Roberts, 1975) because the GPS-PWV does not have a normal distribution. Additionally, the statistical significance of each correlation was evaluated by rejecting the hypothesis of a null correlation when  $p < 5\%$  significance level.

The histograms presented in Figure 8 indicate that the GPS-PWV crests are more frequent in the interval between 15 and 30 min before maximum precipitation occurs (39% of the cases evaluated), and 85% of the positive correlations occurred between 15 and 60 min. After the rainfall events, when the GPS-PWV decreased, the time lag observed was between 15 and 60 min. In 50% of the cases, the minimum GPS-PWV occurred between 45 and 60 min. As already mentioned, several mechanisms can be responsible for the PWV decrease, and the specific physical process for each event can vary. This result corroborates the pattern observed in Figure 3, which shows the GPS-PWV maximum before the precipitation event and its minimum after the maximum precipitation, which indicates a conceptual model that can be explored for nowcasting applications.

### 4.3 | GPS-PWV-derivative analysis: the potential for nowcasting application

Iwabuchi *et al.* (2006), Shi *et al.* (2015) and Benevides *et al.* (2015) suggest a maximum threshold of the GPS-PWV time

derivation to predict a rainfall event. However, the results reported by wavelet analysis demonstrated a very complex process and a more elaborate model should be employed to predict a rainfall event instead of a single threshold. The intensity of the precipitation event is highly correlated with the intensity of the PWV time derivation and the PWV absolute value, which is formed by a succession of pulses of positive increases in the PWV, which compose the GPS-PWV jumps. Therefore, the GPS-PWV signal, before the occurrence of intense rain events, should be detected by analysing the PWV-GPS time-derivation distribution in an appropriated time window. The size of the time window suggested in this study is 80 min (96 to 16 min before the maximum precipitation). This time window was selected because it contains the GPS-PWV jumps, the peaks of maximum PWV (85% of the cases, as shown by time-lag correlation analysis) and the last and stronger positive pulses of the PWV that compose these jumps. The last 16 min before the precipitation was not used to evidence the potential nowcasting of these results. This period before the precipitation event occurred on DoY 341 is illustrated by the grey box in Figure 3.

The histogram of the GPS-PWV time derivation before precipitation events of different intensities were analysed as a function of the area fraction. Figure 9 shows the distribution of the GPS-PWV time derivative for the period 96 to 16 min before the maximum precipitation peak for the

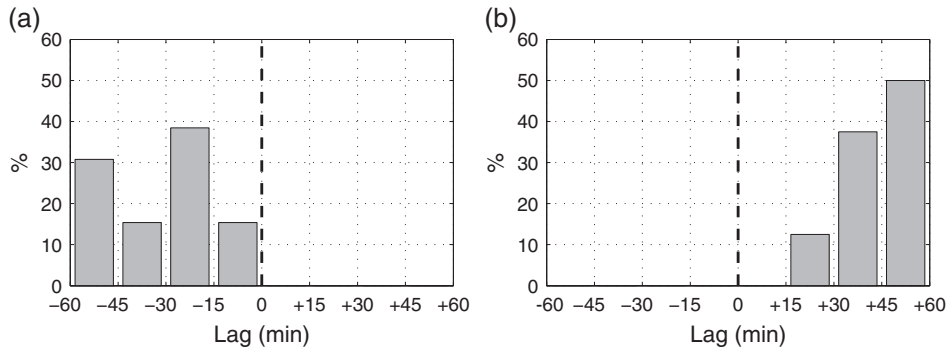


**FIGURE 8** Spearman correlation histograms of maximum positive (a) and minimum negative (b) correlations as functions of the lag of occurrence for Global Positioning System precipitable water vapour (GPS-PWV) values and precipitation events. All 18 precipitation events listed in Table 2 were taken into account in this analysis

18 evaluated events for different terciles of rain fraction (> 35 mm/hr). This precipitation threshold was employed because it has been shown to be the lowest threshold (among the three tested) of rainfall intensity evaluated that presents a significant WCC between the GPS-PWV and precipitation in this time window. Table 2 lists the rainfall events in the terciles and the precipitation fraction observed using the XPol radar during the maximum precipitation peak for each event. In Figure 2d, each event can be visualized by observing the respective DoY. The same calculation was conducted for periods with rainfall events of intensities < 20 mm/hr including periods without observed precipitation, which is labelled in Figure 9 as “Other cases.” The derivatives were calculated every 1 min using  $\Delta t = 6$  min. This interval was selected because it is the sampling rate of the precipitation observed using the XPol radar. The statistical metrics of the derivative for different terciles of the precipitation extension are shown in Table 3.

Figure 9 clearly shows a strong change in the pattern of the derivative distribution as a function of the different precipitation extension terciles. In the period without significant rain, the derivative frequency distribution is like a Gaussian distribution with an average of zero and a standard deviation (SD) of 2.5 mm/hr. However, the average of the derivative increases when the precipitation fraction increases, and the peak of the maximum GPS-PWV time derivation moves to positive values as the rainfall terciles increases. Notably, this effect is evident for the middle and upper rainfall terciles and is nearly undetectable for the lower terciles. For the lower terciles, associated with moderate rainfall events, the time derivation histogram is closer to the non-rainfall or reduced-area rain events. This pattern impacts strongly the average GPS-PWV time-derivation values, which change from 0.2 to 0.4 mm/hr for the lower and middle terciles respectively to 2.0 mm/hr for the upper tercile.

The GPS-PWV time-derivation analysis showed that most of the positive derivative frequencies occur before the maximum GPS-PWV peak. The positive derivative > 9.5 mm/hr increases more substantially before rainfall events in the upper tercile (8.8%) than for events in the middle (0.6%) and lower terciles, which are not observed. These changes in GPS-PWV are associated with the positive pulses of the PWV before intense-extensive rainfall events, as discussed in the previous analysis. Figure 10 shows the case-to-

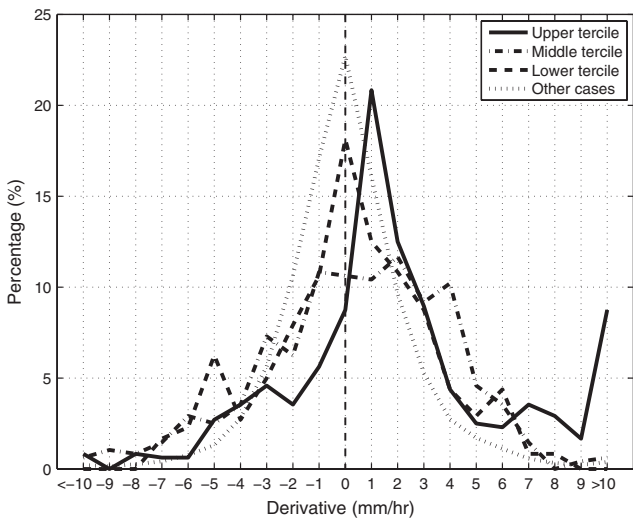


**FIGURE 9** Frequency polygons of the Global Positioning System precipitable water vapour (GPS-PWV) derivatives calculated over the period of 96 to 16 min before the maximum peak of precipitation events for different terciles of the precipitation fraction > 35 mm/hr observed using the XPol radar

**TABLE 3** Statistical measurements of the Global Positioning System precipitable water vapour (GPS-PWV) derivative for different extension terciles of precipitation events

Statistical measurements	Other cases	Terciles		
		Lower	Middle	Upper
Average (mm/hr)	0.04	0.20	0.43	2.01
Standard deviation (mm/hr)	±2.52	±3.11	±3.59	±4.42
Median (mm/hr)	0.00	0.14	0.70	1.34
Maximum (mm/hr)	21.13	8.42	11.00	13.25
Minimum (mm/hr)	-19.07	-6.99	-11.54	-12.35
% > 9.5 mm/hr	0.21%	0.00%	0.62%	8.75%
% < -9.5 mm/hr	0.38%	0.00%	0.62%	0.83%

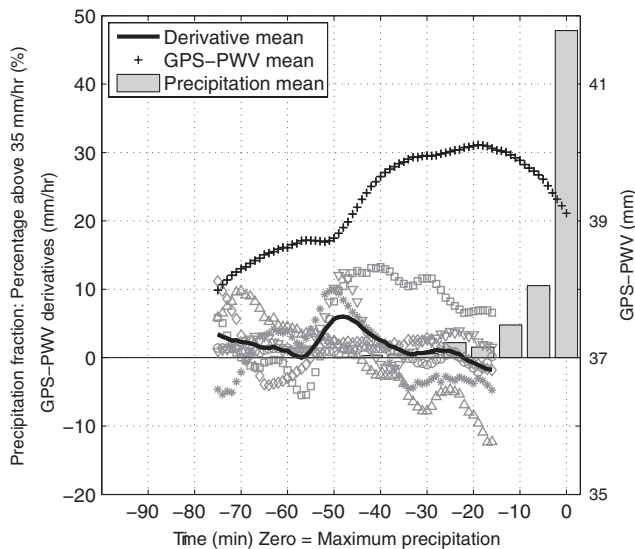


**FIGURE 10** Time series of the Global Positioning System precipitable water vapour (GPS-PWV) derivative before precipitation for upper terciles. The means of the GPS-PWV derivative, precipitation and GPS-PWV for these events are also shown

case events of the upper terciles and the composite time series of the GPS-PWV time derivation normalized by rainfall time. It shows that the GPS-PWV composite configured the PWV jump with a peak 20 min before maximum precipitation and the 60% of total precipitation was observed in the last 10 min of the time window used. The GPS-PWV time-derivation values' mean is positive from 96 to 22 min before the maximum precipitation with three local maximums (28, 49 and 79 min before maximum precipitation). These local maximums are affected by positive pulses of the GPS-PWV (derivative  $> 9.5$  mm/hr), which are observed in five events (85% of the cases) contained in the upper tercile. In other words, this result indicates that the monitoring of the increase in the population of the GPS-PWV derivatives  $> 9.5$  mm/hr can be explored for future application to nowcasting.

Haan and Holleman (2009) reported the construction and validation of a real-time PWV map from a GPS network combined with data from weather radar, a lightning-detection network and surface wind observations. They tested a nowcasting algorithm for three thunderstorm case studies and concluded that the GPS-PWV in real time can be helpful for the nowcasting of severe thunderstorms. Shi *et al.* (2015) studied the PWV estimates in real time for rainfall monitoring and forecasting and showed that this estimate has quality comparable with a post-processed product. A significant reduction in latency was obtained with the GPS data processing proposed by Shi *et al.* (2015), which demonstrated a promising perspective of the PWV-GPS data for rainfall forecasting. The results presented in this study confirm the huge potential of the use GPS-PWV jump characteristics when employed in nowcasting.

## 5 | CONCLUSIONS

This work evaluates the relationship between large and rapid increases in the Global Positioning System precipitable water vapour (GPS-PWV) and the occurrence of rainfall events observed by radar during the CHUVA Vale experiment in Brazil. A detailed analysis of the GPS-PWV time series was carried out, and a strong and sudden sharp increase composed predominantly of positive derivatives before the precipitation events were identified was called GPS-PWV “jumps.” In this process, a crest in the PWV series (composed by several positive pulses of PWV) is remarkable before the precipitation events. Although this sharp increase can be observed for any precipitation event, it is preponderant before more intense and extensive precipitation events.

The wavelet analysis for the GPS-PWV time series was explored to characterize the strong changes in the power spectrum between different timescales during precipitation events generated by the occurrence of the GPS-PWV jumps. Additionally, the application of the wavelet cross-correlation (WCC) between the PWV and precipitation showed that important oscillations exist between these variables on the scale related to a period between 32 and 64 min (associated with GPS-PWV jumps) and between 16 and 34 min (associated with positive pulses of PWV), which is stronger for events of large intensity and extension.

A time-lag correlation histogram shows that in 85% of the studied events, a crest in the PWV time series occurs between 15 and 60 min before the maximum precipitation. The GPS-PWV derivative histogram shows the distribution change for different precipitation extension terciles. The averages of the GPS-PWV derivatives present an increase in positive values as a function of the increase in the rainfall extension terciles. The results suggest that the derivative averages in the interval of 96 to 16 min before precipitation changes to positive values (2 mm/hr) influenced by the GPS-PWV jump, and an increase in the frequency of the high GPS-PWV time-derivation values ( $> 9.5$  mm/hr associated with positive pulses of PWV) indicates the preminent event of intense to torrential precipitation. There is a clear GPS-PWV time-derivation pattern that can be explored for use in nowcasting applications.

## ACKNOWLEDGEMENTS

The authors are grateful for discussions with David Adams. Thanks to the members of the CHUVA team who were involved directly or indirectly in the data collection by XPol radar, disdrometer and Global Positioning System (GPS) receiver during the CHUVA Vale experiment in São José dos Campos-S.P. Special thanks to Thiago Souza Biscaro. This study was directly supported by the Fundação de Amparo à Pesquisa do Estado de São Paulo (FAPESP)

(grant process numbers 2009/15235-8 and 2015/14497-0) and by the Contractual Instrument of the Thematic Network of Geotectonic Studies CT-PETRO (PETROBRAS) and Instituto Nacional de Pesquisas Espaciais (INPE) (grant number 600289299), which provided the GPS receiver used. The raw data (Level 0) used from the XPol radar, disdrometer and GPS receiver and the values obtained by applying the methodology reported in Section 2 (Level 2) are freely available through the Brazilian Institute for Space Research (see <ftp://pararaca.cptec.inpe.br/>) after registration in the CHUVA Project portal (see <http://chuvaproject.cptec.inpe.br>).

## ORCID

Luiz F. Sapucci  <https://orcid.org/0000-0001-8420-8033>

## REFERENCES

- Adams, D.K., Fernandes, R.M.S., Kursinski, E.R., Maia, J.M., Sapucci, L.F., Machado, L.A.T., Vitorello, I., Monico, J.F.G., Holub, K.L., Gutman, S.I., Filizola, N. and Bennett, R.A. (2011) A dense GNSS meteorological network for observing deep convection in the Amazon. *Atmospheric Science Letters*, 12, 207–212.
- Adams, D.K., Gutman, S.I., Holub, K.L. and Pereira, D.S. (2013) GNSS observations of deep convective time scales in the Amazon. *Geophysical Research Letters*, 40, 2818–2823.
- Bastin, S., Champollion, C., Bock, O., Drobinski, P. and Masson, F. (2005) On the use of GPS tomography to investigate water vapor variability during a mistral/sea breeze event in southeastern France. *Geophysical Research Letters*, 32, L05808.
- Benevides, P., Catalao, J. and Miranda, P.M.A. (2015) On the inclusion of GPS precipitable water vapour in the nowcasting of rainfall. *Natural Hazards and Earth System Sciences*, 15, 2605–2616.
- Bennett, G. and Jupp, A. (2012) Operational assimilation of GPS zenith total delay observations into the Met Office numerical weather prediction models. *Monthly Weather Review*, 140, 2706–2719.
- Best, D.J. and Roberts, D.E. (1975) Algorithm AS 89: the upper tail probabilities of Spearman's rho. *Journal of the Royal Statistical Society*, 24, 377–379.
- Bevis, M., Chiswell, G., Herring, T.A., Anthes, R., Rocken, C. and Ware, E.R. H. (1994) GPS meteorology: mapping zenith wet delays into precipitable water. *Journal of Applied Meteorology*, 33, 379–386.
- Bevis, M., Susinger, S., Herring, T., Rocken, C., Anthes, R.A. and Ware, R. (1992) GPS meteorology: remote of atmospheric water vapor using the Global Positioning System. *Journal of Geophysical Research*, 97, 15787–15801.
- Bock, O., Bouin, M.N., Doerflinger, E., Collard, P., Masson, F., Meynadier, R., Nahmani, S., Koité, M., Gaptia Lawan Balawan, K., Didé, F., Ouedraogo, D., Pokperlaar, S., Ngamini, J.B., Lafore, J.P., Janicot, S., Guichard, F. and Nuret, M. (2008) The West African Monsoon observed with ground-based GPS receivers during AMMA. *Journal of Geophysical Research*, 113, D21105.
- Boehm, J., Werl, B. and Schuh, H. (2006) Troposphere mapping functions for GPS and VLBI from ECMWF operational analysis data. *Journal of Geophysical Research*, 111, B02406.
- Brenot, H., Walpersdorf, A., Reverdy, M., van Baelen, J., Ducrocq, V., Champollion, C., Masson, F., Doerflinger, E., Collard, P. and Giroux, P. (2014) A GPS network for tropospheric tomography in the framework of the Mediterranean hydrometeorological observatory C evennes-Vivarais (southeastern France). *Atmospheric Measurement Techniques*, 7, 553–578.
- Bringi, V.N., Thurai, M. and Hanesen, R. (2005) *Dual-Polarization Weather Radar Handbook*, 2nd ed. Neuss, 163 pp.
- Calheiros, A.J.P. and Machado, L.A.T. (2014) Cloud and rain liquid water statistics in the CHUVA campaign. *Atmospheric Research*, 144, 126–140.
- Chan, P.W. (2009) Performance and application of a multi-wavelength, ground-based microwave radiometer in intense convective weather. *Meteorologische Zeitschrift*, 18, 253–265.
- Cucurull, L., Vandenbergh, F., Barker, D., Vilaclara, E. and Rius, A. (2004) Three-dimensional variational data assimilation of ground-based GPS ZTD and meteorological observations during the 14 December 2001 storm event over the Western Mediterranean Sea. *Monthly Weather Review*, 132, 749–763.
- Daubechies, I. (1992) *Ten Lectures on Wavelets*. Philadelphia, PA: Society for Industrial and Applied Mathematics. <https://doi.org/10.1137/1.9781611970104>.
- Davis, J.L., Herring, T.A., Shapiro, I., Rogers, A.E. and Elgened, G. (1985) Geodesy by radio interferometry: effects of atmospheric modeling errors on estimates of baseline length. *Radio Science*, 20, 1593–1607.
- Giangrande, S.E., Toto, T., Bansemir, A., Kumjian, M.R., Mishra, S. and Ryzhkov, A.V. (2016) Insights into riming and aggregation processes as revealed by aircraft, radar, and disdrometer observations for a 27 April 2011 widespread precipitation event. *Journal of Geophysical Research – Atmospheres*, 121, 5846–5863.
- Gregorius, T. (1996) *GIPSY-OASIS II How it works*. Department of Geomatics, University of Newcastle upon Tyne; 167. Available at: <http://web.gps.caltech.edu/classes/ge167/file/gipsy-oasisIIHowItWorks.pdf> [Accessed 15th September 2017].
- Guerova, G., Jones, J., Dousa, J., Dick, G., De Haan, S., Pottiaux, E., Bock, O., Pacione, R., Elgered, G., Vedel, H. and Bender, M. (2016) Review of the state-of-the-art and future prospects of the ground-based GNSS meteorology in Europe. *Atmospheric Measurement Techniques Discussions*, 9, 5385–5406.
- Haan, S.D. (2006) Measuring atmospheric stability with GPS. *Journal of Applied Meteorology and Climatology*, 45, 467–475.
- Haan, S.D., Barlag, S., Baltink, H.K., Debie, F. and Marel, H.V. (2004) Synergistic use of GPS water vapor and Meteosat images for synoptic weather forecasting. *Journal of Applied Meteorology*, 43, 514–518.
- Haan, S.D. and Holleman, I. (2009) Real-time water vapor maps from a GPS surface network: construction, validation, and applications. *Journal of Applied Meteorology and Climatology*, 48, 1302–1316.
- Holloway, C. and Neelin, J. (2010) Temporal relations of column water vapor and tropical precipitation. *Journal of the Atmospheric Sciences*, 67, 1091–1105.
- IERS Conventions. (2010) Gérard Petit and Brian Luzum (Eds). *IERS Technical Note: 36*. Frankfurt am Main: Verlag des Bundesamts für Kartographie und Geodäsie; p. 179. ISBN 3-89888-989-6. Available at: <https://www.iers.org/IERS/EN/DataProducts/Conventions/conventions.html> [Accessed 15th September 2017].
- Iwabuchi T, Rocken C, Lukes Z, Mervat L, Johnson J, Kanzaki M. (2006) PPP and network true real-time 30 sec estimation of ZTD in dense and giant regional GPS network and the application of ZTD for nowcasting of heavy rainfall. *Proceedings of the 19th International Technical Meeting of the Satellite Division of The Institute of Navigation (ION GNS 2006)*, 26–29 September 2006, Fort Worth, TX, Manassas, VA: Institute of Navigation, pp. 1902–1909.
- Jerrett, D. and Nash, J. (2001) Potential uses of surface based GPS water vapour measurements for meteorological purposes. *Physics and Chemistry of the Earth*, 26, 457–461.
- Joss, J. and Waldvogel, A. (1967) Ein Spektrograph für Niederschlags-tropfen mit automatischer Auswertung (A spectrograph for rain drops with automatic analysis). *Pure and Applied Geophysics*, 68, 240–246.
- Kinnell, P.I.A. (1976) Some observations on the Joss-Waldvogel rainfall disdrometer. *Journal of Applied Meteorology*, 15, 499–502.
- Kursinski, E.R., Bennett, R.A., Gochis, D., Gutman, S.I., Holub, K.L., Mastaler, R., Minjarez Sosa, C., Minjarez Sosa, I. and van Hove, T. (2008) Water vapor and surface observations in northwestern Mexico during the 2004 NAME enhanced observing period. *Geophysical Research Letters*, 35, L03815.
- Lindzen, R.S. and Tung, K-K. (1976) Banded convective activity and ducted gravity waves. *Monthly Weather Review*, 104, 1602–1617. [https://doi.org/10.1175/1520-0493\(1976\)104<1602:BCAADG>2.0.CO;2](https://doi.org/10.1175/1520-0493(1976)104<1602:BCAADG>2.0.CO;2).
- Lyard, F., Lefèvre, F., Letellier, T. and Francis, O. (2006) Modelling the global ocean tides: a modern insight from FES2004. *Ocean Dynamics*, 56, 394–415.
- Machado, L.A.T., Silva Dias, M.A.F., Morales, C., Fisch, G., Vila, D., Albrecht, R., Goodman, S.J., Calheiros, A.J.P., Biscaro, T., Kummerow, C., Cohen, J., Fitzjarrald, D., Nascimento, E.L., Sakamoto, M.S., Cunningham, C., Chaboureaud, J.P., Petersen, W.A., Adams, D.K., Baldini, L., Angelis, C.F., Sapucci, L.F., Salio, P., Barbosa, H.M.J.,

- Landulfo, E., Souza, R.A.F., Blakeslee, R.J., Bailey, J., Freitas, S., Lima, W. F.A. and Tokay, A. (2014) The Chuva project: how does convection vary across Brazil. *Bulletin of the American Meteorological Society*, 95, 1365–1380.
- Madhulatha, A., Rajeevan, M., Venkat Ratnam, M., Bhate, J. and Naidu, C.V. (2013) Nowcasting severe convective activity over southeast India using ground-based microwave radiometer observations. *Journal of Geophysical Research*, 118, 1–13.
- Mazany, R.A., Businger, S., Gutman, S.I. and Roeder, W. (2002) A lightning prediction index that utilizes GPS integrated precipitable water vapor. *Weather and Forecasting*, 17, 1034–1047.
- Montenbruck, O., Schmid, R., Mercier, F., Steigenberger, P., Noll, C., Fatkulin, R., Kogure, S. and Ganeshan, A.S. (2015) GNSS satellite geometry and attitude models. *Advances in Space Research*, 56, 1015–1029.
- Moore, A., Small, I., Gutman, S., Bock, Y., Dumas, J., Fang, P., Haase, J., Jackson, M. and Laber, J. (2015) National Weather Service Forecasters use GPS precipitable water vapor for enhanced situational awareness during the Southern California Summer Monsoon. *Bulletin of the American Meteorological Society*, 96, 1867–1877.
- Muller, C.J., Back, L.E., O’Gorman, P.A. and Emanuel, K.A. (2009) A model for the relationship between tropical precipitation and column water vapor. *Geophysical Research Letters*, 36, L16804.
- Raymond, D.J. (1987) A forced gravity wave model of self-organizing convection. *Journal of the Atmospheric Sciences*, 44, 3528–3543.
- Rocken, C., VanHove, T., Rothacher, M., Solheim, F., Ware, R., Bevis, M., Businger, S. and Chadwick, R. (1994) Towards near-real-time estimation of atmospheric water vapor with GPS. *Eos Transactions American Geophysical Union*, 7544. (Fall Meet Suppl), 173.
- Sapucci, L.F. (2014) Evaluation of modeling water-vapor-weighted mean tropospheric temperature for GNSS-integrated water vapor estimates in Brazil. *Journal of Applied Meteorology and Climatology*, 53, 715–730.
- Sapucci, L.F., Machado, L.A.T., Monico, J.F.G. and Plana-Fattori, A. (2007) Intercomparison of integrated water vapor estimative from multi-sensor in Amazonian regions. *Journal of Atmospheric and Oceanic Technology*, 24, 1880–1894.
- Sato, T. and Kimura, F. (2005) Diurnal cycle of convective instability around the Central Mountains in Japan during the warm season. *Journal of Atmospheric Sciences*, 62, 1626–1636.
- Schmid, R., Steigenberger, P., Gendt, G., Ge, M. and Rothacher, M. (2007) Generation of a consistent absolute phase-center correction model for GPS receiver and satellite antennas. *Journal of Geodesy*, 81, 781–798.
- Serra Yolande, L., Adams, D.K., Minjarez-Sosa, C., Moker, J.M., Arellano, A., Jr., Castro, C., Quintanar, A. and DeMets, C. (2016) The North American monsoon GPS transect experiment 2013. *Bulletin of the American Meteorological Society*, 97, 2103–2115.
- Shangguan, M., Heise, S., Bender, M., Dick, G., Ramatschi, M. and Wickert, J. (2015) Validation of GPS atmospheric water vapor with WVR data in satellite tracking mode. *Annales de Geophysique*, 33, 55–61.
- Shi, J., Chaoqian, X., Jiming, G. and Yang, G. (2015) Real-time GPS precise point positioning-based precipitable water vapor estimation for rainfall monitoring and forecasting. *IEEE Transactions on Geoscience and Remote Sensing*, 53, 3452–3459.
- Solheim, F.S., Vivekanandan, J., Ware, R.H. and Rocken, C. (1999) Propagation delays induced in GPS signals by dry air, water vapor, hydrometeors, and other particulates. *Journal of Geophysical Research*, 104, 9663–9670.
- Testud, J., Bouar, E.L., Obligis, E. and Ali-Mehenni, M. (2000) The rain profiling algorithm applied to polarimetric weather radar. *Journal of Atmospheric and Oceanic Technology*, 17, 332–356.
- Whitcher, P., Guttorp, D.B. and Percival, B. (2000) Wavelet analysis of covariance with application to atmospheric time series. *Journal of Geophysical Research*, 105, 14941–14962.
- Wolfe, D.E. and Gutman, S.I. (2000) Developing an operational, surface-based, GPS, water vapor observing system for NOAA: network design and results. *Journal of Atmospheric and Oceanic Technology*, 17, 426–440.
- Zumberge, J.F., Heflin, M.B., Jefferson, D.C., Watkins, M.M. and Webb, F.H. (1997) Precise point positioning for the efficient and robust analysis of GPS data from large networks. *Journal of Geophysical Research*, 102(B3), 5005–5017.

## SUPPORTING INFORMATION

Additional supporting information may be found online in the Supporting Information section at the end of the article.

**How to cite this article:** Sapucci LF, Machado LAT, de Souza EM, Campos TB. Global Positioning System precipitable water vapour (GPS-PWV) jumps before intense rain events: A potential application to nowcasting. *Meteorol Appl.* 2018;1–15. <https://doi.org/10.1002/met.1735>